INDERSCIENCE PUBLISHERS
Linking academia, business and industry through research

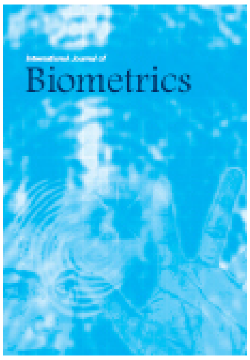

International Journal of Biometrics

ISSN online: 1755-831X - ISSN print: 1755-8301
https://www.inderscience.com/ijbm

A secure finger vein recognition system using WS-progressive GAN and C4 classifier

R. Sreemol, M.B. Santosh Kumar, A. Sreekumar

DOI: 10.1504/IJBM.2024.10053719

Article History:

Received:	30 December 2021
Last revised:	23 December 2022
Accepted:	23 December 2022
Published online:	01 December 2023

A secure finger vein recognition system using WS-progressive GAN and C4 classifier

R. Sreemol*

Department of Computer Applications,
Cochin University of Science and Technology,
South Kalamassery, Kochi,
Kerala, India
Email: sreemolr@cusat.ac.in
*Corresponding author

M.B. Santosh Kumar

Division of IT,
School of Engineering,
Cochin University of Science and Technology,
South Kalamassery, Kochi,
Kerala, India
Email: santo_mb@cusat.ac.in

A. Sreekumar

Department of Computer Applications,
Cochin University of Science and Technology,
South Kalamassery, Kochi,
Kerala, India
Email: sreekumar@cusat.ac.in

Abstract: This paper proposes a secure finger vein reconstruction and recognition system utilising a novel weight standardisation-based progressive generative adversarial networks (WS-progressive GAN) as well as 'he' initialised chimp optimisation-based convolutions neural network (he-ChOA-CNN) classifier for overcoming security issues. Initially, the input images are pre-processed, and the reflection-based contrast limited adaptive histograms equalisation (RCLAHE) enhanced the pre-processed images. Next, bias locality-sensitive hashing (BLSH) generates hash values, through which the ameliorated images are secured. Next, the secured images are augmented and applied for WS-progressive GAN, which encodes and decodes the image for reconstructing the synthetic images. Then, the he-ChOA-CNN accepts the imperative features extracted as of the synthetic images as input for training. Amid testing, the identity of the person is recognised utilising the classifier output and the query image by detecting the gaps. Analogised to the prevailing methods, more accurate outcomes are attained by the proposed model, which is illustrated through the experimental outcomes.

Keywords: reflection-based contrast limited adaptive histogram equalisation; finger vein; bias locality-sensitive hashing; BLSH; he initialisation; chimp optimisation-based CNN; generative adversarial network; progressive GAN.

Reference to this paper should be made as follows: Sreemol, R., Santosh Kumar, M.B. and Sreekumar, A. (2024) 'A secure finger vein recognition system using WS-progressive GAN and C4 classifier', *Int. J. Biometrics*, Vol. 16, No. 1, pp.44–67.

Biographical notes: R. Sreemol received her Bachelor's in Computer Science and Engineering in 2014 and Master's in Computer Science and Engineering in 2017, where she is currently pursuing her PhD from the Department of Computer Applications, Cochin University of Science and Technology, South Kalamassery, Kochi, Kerala, India. Her research interests include pattern recognition and image processing with applications in biometrics and security systems.

M.B. Santosh Kumar received his PhD in Development of Innovative Procedures for Information Technology Articulated Agriculture in 2018 from the Cochin University of Science and Technology, South Kalamassery, Kochi, Kerala, India. He is an Associate Professor at Division of IT, School of Engineering, CUSAT. He has granted a patent on 'Portable Agriculture Network System' on 2017. His research interests are related to knowledge-based systems in agriculture and AI in agriculture.

A. Sreekumar received his PhD in Cryptography from the Cochin University of Science and Technology, South Kalamassery, Kochi, Kerala, India in 2010. He joined as a Lecturer in Department of Computer Applications, CUSAT and currently working as Professor. He has 29 years of teaching experience. His research interest is in cryptography, number theory and secret sharing.

1 Introduction

Diverse technologies like digital signatures, watermarking, biometric (BM) recognition and many are rising owing to the decisive requirement for authentication methods to protect digital information and user identity (Kapoor et al., 2021). The conventional identity techniques like smart cards, passwords as well as signatures are now no more the finest choices (Noh et al., 2020). Via greater anti-spoof capacities, BM is considerably enhanced (Hu et al., 2020) which led to more consistent, protected, and suitable authentication (Yang et al., 2020). To protect private information, identification, and validation, the BM-based recognition technique is employed (Ren et al., 2021). Face, iris, fingerprint, FV, palm vein, voiceprint, gait and signature are the diverse technologies used in it (Song et al., 2019). Detection of the living body, compact device size, and excellent safety is the clear benefits of hand and FV systems when compared with other BMs (Zhao et al., 2020). For numerous applications, the FV systems have been verified to be a viable substitute to finger-based systems (Zhang et al., 2019).

The interest in the usage of finger vascular (also called FV) pattern as a BM modality has been grown owing to the requirement for dependable together with precise authentication in safe applications (Ramachandra et al., 2019). Border crossing control, attendance systems, and financial safety are many BM technology applications. At present, fingerprint recognition is built into every smartphone. FV authentication is extensively available in all smart devices, apart from face and iris authentication (Kirchgasser et al., 2020). On comparing with the other traditional methods, the boon of FV-based systems is that it is non-intrusive (Fairuz et al., 2019a) and duplication of FV information is very complex (Fairuz et al., 2019b). The enriched secrecy during personal authentication is another benefit of using the FV image-based identification because the subsurface vascular patterns are greatly concealed beneath; and under visible illumination, it is complex to steal the image (Xie and Kumar, 2019). The FV recognition has several feature extraction techniques, which can well be classified as follows. The segmented blood vessel pattern or minutiae has been utilised to categorise FV images in Vein pattern-based methodology (Liu et al., 2019a). The cross, as well as endpoints, are illustrated as minutiae in minutiae-based techniques and as per the surrounding local features, they compute their similarity. The features are collected from segmented blood vessels by the network-based approaches, and in line with the distribution of the vessel structures, they are matched (Meng et al., 2020).

But when the BM template is compromised or stolen, privacy invasion and impersonation might happen, in spite of the BMs outstanding utility in the authentication. The BM characters are irreversible and incomparable, so this may lead to more complications (Muthusamy and Rakkimuthu, 2021a). With the help of diverse strategies, more investigation work has been constructed in prevailing work for FV verification along with protection of template (Liu et al., 2019b). But, the identification of FV features in raw images is not robust. As a result, employing a WS-progressive GAN and he-ChOA-CNN classifier, a secure FV reconstruction and identification system is proposed in this work. Table 1 include the overview of the notions used in this work.

The remaining of the paper is structured as follows: Section 2 describes the proposed finger vein recognition system (FRS), Section 3 details the experimentation results and Section 4 concludes the paper with future work.

1.1 Our contributions

The main contributions of this research are as follows:

- To propose an efficient pre-processing technique for improving the classification accuracy and reducing the processing time.
- To present the reflection-based contrast limited adaptive histogram equalisation (RCLAHE) for contrast enhancement (CE).
- To improve the classification using Chen chaotic chimp with convolutional neural network (C4) for avoiding the vanishing gradient problems.
- To introduce the bias locality-sensitive hashing (BLSH) for performing the biometric input data security and key generation.
- To present the weight standardisation-progressive GAN (WS-progressive GAN).
- To compare the proposed technique with the existing technique using various result parameters and existing algorithms.

Table 1 Overview of our notions

Notions	*Meaning*
ANN	Artificial neural network
BLSH	Bias locality-sensitive hashing
BM	Biometric
CDF	Cumulative distributions function
CE	Contrast enhancement
CL	Convolution layer
CLAHE	Contrast limited adaptive histogram equalisation
CNN	Convolution neural networks
ChOA	Chimp optimisation algorithm
CSO	Crow search optimisation
DCNN	Deep convolution neural networks
FCL	Fully connected layer
FDR	False discovery rate
FM	Feature map
FNR	False negative rate
FP	Fingerprint, false positive
FPR	False positive rate
FRR	False recognition rate
FV	Finger vein
GAN_CNN	Generative adversarial networks-based CNN
He-ChOA	'He' initialised chimp optimisation algorithm
HF	Hash function
HHO	Harish Hawks optimisation
LBP	Local binary pattern
LLBP	Local line binary pattern
MCC	Mathews correlation coefficient
NPV	Negative predictive value
PHDCP	Pyramid histogram of double competitive pattern
PL	Pooling layer
PSNR	Pixel signal to noise ratio
RCLAHE	Contrast limited adaptive histograms equalisation
ReLU	Rectified linear activation function
RNN	Recurrent neural networks
RSO	Rat swarm optimisation
SIFT	Scale-invariants feature transform
SSIM	Structure similarity index measure
TP	True-positive
TN	True-negative
WS-progressive GAN	Weight standardisation-based progressive GAN

2 Proposed FRS

Considerable attention is drawn by the biometric systems with augmenting growth in the demand for security. Nevertheless, most biological patterns are susceptible to spoofing attacks. More user-friendly, lower-cost, and extremely secure biological patterns, say palmvein together with FV, have attained much attention. It is because they belong to the intrinsic modalities within humans' bodies and are hard to forge. The FV imaging device, in contrast to palm-vein, is more fine and simple to assemble which makes FV recognition technology conducive to popularise. Therefore, an effectual FV recognition system utilising a WS-progressive GAN in addition to he-ChOA-CNN is proposed.

Figure 1 Block diagram of the proposed methodology (see online version for colours)

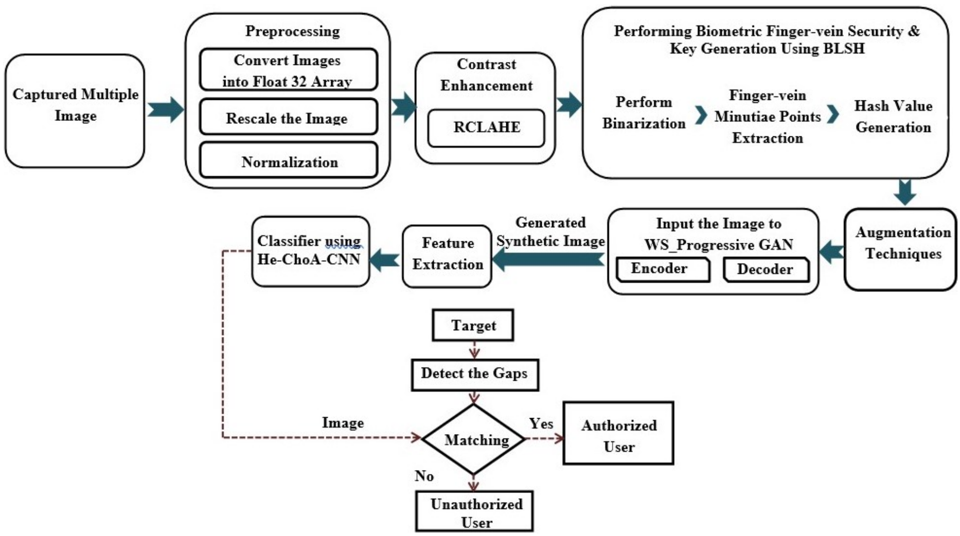

The proposed method's block diagram is exhibited in Figure 1. Pre-processing, CE, security and key generation, augmentation techniques, WS-progressive GAN, feature selection, and C4 classification are the seven stages that are involved in the proposed work. Initially, the inputted FV images are pre-processed and implemented to reflection-based contrast limited adaptive histogram equalisation (RCLAHE) for CE. Next, BLSH takes care of the security as well as the key generation process for the ameliorated images. Then, the secured images are augmented and reconstructed as synthetic images utilising the encoder together with the decoder in the WS-progressive GAN. The vital features are extracted as of the synthetic images, which are inputted to the He-ChOA-CNN that outputs it as an authorised or non-authorised user.

2.1 Pre-processing

The initial step of the proposed system is pre-processing. It totally consists of three steps: converting the multiple FP images into float 32 array, rescaling the images, along with normalisation. The input images are initialised as:

$$W_{fp(n)} = \{W_{fp(1)}, W_{fp(2)}, W_{fp(3)}, ..., W_{fp(N)}\} \tag{1}$$

wherein $W_{(n)}$ signifies the total input images. At first, the input images are transmuted into a float-32 array. It can well be expressed as,

$$arr(W_{fp(n)}) = Float32Array(W_{fp(n)}) \tag{2}$$

wherein $Float32Array(.)$ signifies the function that signifies an array of 32-bit floating-point numbers, $arr(W_{fp(n)})$ implies the float-32 arrays subsequent to conversion. Next, for creating a new version of the image with disparate sizes utilising the scaling factor, the converted images are rescaled. The rescaled images are attained as:

$$rs(W_{fp(n)}) = \zeta(arr_{(W_{fp(n)})}) \tag{3}$$

where $rs(W_{fp(n)})$ implies the total rescaled images, ζ signifies the scaling factor. Next, for converting the image to a range of pixel values, the rescaled images are normalised. The normalised images are signified as $norm(W_{fp(n)})$. Thus, the pre-processed image $W_{pp(n)}$ are implied as:

$$W_{pp(n)} = \{W_{pp(1)}, W_{pp(2)}, W_{pp(3)}, ..., W_{pp(N)}\} \tag{4}$$

2.2 Contrast enhancement

FP image enhancement is an important step. The quality to accurately detect adequate reliable features, namely, minutiae and FP singularities will be enhanced. The pre-processed images $W_{pp(n)}$ are implemented to the RCLAHE (Muthusamy and Rakkimuthu, 2021b) for CE. CLAHE functions on smaller regions on the image, termed tiles, instead of the complete image. It is basically a variation of adaptive histogram equalisation. For removing the artificial boundaries, the neighbouring tiles are joined utilising bilinear interpolation. The reflection technique is incorporated in the prevailing CLAHE for ameliorating the image's CE. The entire region of the image and the portion of the image flipped over one or the other portions of the image by including a negative sign is reviewed by the reflection-based transformation function. This aids to concentrate on the whole region of the image intended for CE. The RCLAHE steps are:

- Manifold regions are split as of every pre-processed image $W_{pp(n)}$ and also the histogram of every region is attained.
- For limiting the amplification, the clip limit (CL) is ascertained to clip the predefined value of the histogram. The CL can well be obtained as:

  $$\chi_{cl} = L_{\max}.O + \frac{O}{O_{\max}}(1 - L_{\max}) \tag{5}$$

  where $L_{\max}$ is the maximum limit of the histogram slope where the pixels ranges from O to $O_{\max}$, χ_{cl} is the CL.
- Next, the histogram equalisation is done for the altered histogram. Here, the clipped pixels are distributed equally to every grey level. The cumulative distributions function (CDF) is computed for histogram equalisation as:

  $$\Omega_{cdf} = \sum_{k=1}^{K} \varrho(W_{pp(n_k)}) \tag{6}$$

  where Ω_{cdf} denotes the CDF function, ϱ denotes the probability for k pixels. Then, the reflection-based transformation function for grey-scale mapping is computed as:

$$R(T_{fun}) = \frac{(N_{gl} - 1).\Omega_{cdf}}{N_p} \tag{7}$$

where $R(T_{fun})$ denotes the reflection-based transformation function across the horizontal $-R(T_{fun})$ and vertical $R(-T_{fun})$ axis.

- Lastly, via interpolating the partitioned regions, the enhanced image is reconstructed. The enhanced image is denoted as $W_{CE(n)}$

2.3 Security and key generation

Following CE, via binarisation along with minutiae extraction, the security phase for securing the BM data is executed; similarly, by utilising the BLSH, the hash code is created. The LSH (Lai et al., 2021) is a hash function (HF) in which it takes a certain data point; subsequently, hashes it into a number. The bias locality is considered in the sensitive hashing algorithm to ameliorate the hash code complexity; here, it permits the HF to be shifted to the left or right to fit the data effectively. Following are the steps incorporated:

- Firstly, the enhanced image $W_{CE(n)}$ is binarised; subsequently, forms the image's skeleton.
- The binary image is thinned for extracting the minutiae points. Due to this, a ridge is just '1' pixel wide.
- The points that comprise a pixel value of one (ridge ending) as their neighbour or more than two ones (ridge bifurcations) in their neighbourhood are called minutiae points. The bifurcations are marked by the proposed work as the minutia points since there is no ridge ending for the FV. The extracted minutia points are exhibited as:

$$mp_i = \{mp_1, mp_2, mp_3, ..., mp_K\} \tag{8}$$

where mp_i denotes the number of minutia points extracted, mp_K denotes the K_{th} minutia point.

- The BLSH hash function accepts the extracted minute points as the input. Centred on the spatiality of the data, it generates hash values.
- In BLSH, m hash functions are chosen independently and uniformly at random. The hash functions are expressed as:

$$H_m[mp_i] = \{H_1[mp_1 + B], H_2[mp_2 + B], ..., H_m[mp_m + B]\} \tag{9}$$

where $H_m[mp_i]$ denotes the m number of hash functions, B denotes the bias added with the minute points. The bias can be computed as:

$$B = \frac{1}{Loc(Loc - 1)} \sum_{i-1}^{Loc} \frac{AC[mp_i]}{Cor[mp_i]} \tag{10}$$

where Loc denotes the locality, AC and Cor denote the auto co-variance and correlation of the minutia points.

- m hash tables are built utilising every HF. All the minutia points are inserted in every hash table via computing respective hash values. The output images subsequent to generating the hash values are signified as $W_{H(n)}$.

2.4 Augmentation techniques

Augmentation (Lu et al., 2021) is a technique wherein the existing data are modified or the dataset accessible for training a learning model is expanded artificially. By the conversion in various directions, the augmentation of the images is executed. Utilising the translation in orientation along with distance, the translation operation is conducted. It is specified as:

$$G = W_{H(n)} | W_{H(n)} = \frac{360^0}{L_G} * i, 1 \leq i \leq L_G \tag{11}$$

$$x = \{W_{H(n)} | 1 \leq W_{H(n)} \leq L_x\} \tag{12}$$

where G denotes the translation orientation containing L_G directions, x denotes the translation distance computed by the pixels. After several translations and augmentation processes, the minutiae finger vein images are obtained and denoted as $W_{A(n)}$.

2.5 WS-progressive GAN

Here, utilising the WS-progressive GAN approach (Huang et al., 2020), the augmented minutiae FV images $W_{A(n)}$ are encoded along with decoded. There are '2' networks pitted against one another in a 2-player game in the progressive GAN, which is a kind of generative model. In the GAN, '2' players are in a steady battle in which one attempts to fool the other, whilst the other attempts not to be fooled. The generator, which trains the encoder net along with generates an image with its code as of certain probability distribution is included in player 1; in addition, it ascertains that they look equivalent to player 2. The image's pixel values are encrypted together with modified by the encoder in numerous ways; subsequently, it produces a random code whereas an image with the arbitrary code is synthesised by the decoder. The discriminator, which trains the decoder net, is included by player 2; it differentiates its inputs and decides whether the inputs are obtained as of the generator or the training distribution. The images are trained in the same manner to attain the synthesised images. In the progressive GAN, a preliminary weight standardisation normalisation is utilised to ameliorate the synthetic images' diversity. Following are steps incorporated in this.

The input parameters are taken by the discriminator, which outputs its discrimination probability via the LF. It is specified as:

$$\psi(\zeta_D, \rho^{Dis}) = A - B \tag{13}$$

where A denotes the data distribution of true samples and B denotes the denotes the data distribution of duplicate samples generated by the generator.

$$A = -T_{W_{A(n)} \sim P_(n)}[\log(\zeta_D . W_{A(n)})] \tag{14}$$

$$B = -T_{W_{A^*(n)} \sim P_(q), c \sim P_(cd)} [\log(1 - \zeta_D(\zeta_G(W_{A^*(q),cd})))] \tag{15}$$

where ψ denotes the loss function, $\log(\zeta_D . W_{A(n)})$ denotes the discriminator output for true samples, q denotes the random noise sampling from a normal distribution $P_{(q)}$, $\log(1 - \zeta_D(\zeta_G(W_{A^*(q),cd})$ denotes the discriminator output for generator outputs. The output of the generator with input parameters $\zeta_G(W_{A^*(q)})$ and ρ^{Gen} can be expressed as:

$$\psi(\zeta_G, \rho^{Gen}) = T_{W_{A^*(n)} \sim P_(Gen), cd \sim P_(c)} [-\log(\zeta_D(\zeta_G(W_{A^*(q),cd})))] \tag{16}$$

where the weight values ρ^{Gen} and ρ^{Dis} are optimised by using weight standardisation normalisation techniques. The weight standardisation is done as:

$$\rho^{"}(Gen, Dis) = \rho' | \rho' = \frac{\rho' - \mu_{mean}(\rho')}{\sigma_{std}(\rho')} \tag{17}$$

where ρ' denotes the weights before standardisation, μ_{mean}, σ_{std} are the mean and standard deviation for each output. Then, the standardised weight vectors are normalised as:

$$\rho^{(Gen,Dis)} = \frac{U}{||\rho^{"}(Gen, Dis)||} \rho^{"}(Gen, Dis) \tag{18}$$

where $\|\rho^{"}(Gen, Dis)\|$ denotes the trainable weight vector that is independent of the parameter U. The generator and discriminator outputs their probability through the logistic sigmoid activation function which can be expressed as:

$$Sig(P_{(n)}, P_{(q)}) = \log \left(\frac{1}{1 + e^{-(P_{(n)}, P_{(q)})}} \right) \tag{19}$$

In the training process, by maximising the LF, the generator executes gradient ascent; similarly, by minimising the LF, the discriminator executes gradient descent. Consequently, for the network, the overall LF is given as:

$$\min_{Gen} \max_{Disc} (\zeta(G), \zeta(D)) = \min_{Ge} \max_{Ds} (A + B) \tag{20}$$

A and B are given by the formulas (14)–(15). When the distribution samples as of the generator congregate to the distribution of real samples as of the discriminator, the global optimum is brought about by the minimax game utilised above. Thus, the reconstructed synthetic images are signified as:

$$W_{syn_{(n)}} = \{W_{syn_{(1)}}, W_{syn_{(2)}}, ..., W_{syn_{(N)}}\} \tag{21}$$

where $W_{syn_{(n)}}$ denotes the the total synthetic images.

2.6 *Feature extraction*

To extract the significant features for training, the reconstructed synthetic images are utilised. The features that are extracted as of the synthetic FP image are local binary pattern (LBP) (Tüű-Szabó et al., 2021), 3D morphable model (Dai et al., 2020), pyramid histogram of double competitive pattern (PHDCP) (Lu et al., 2018), along with local line binary pattern (LLBP) (Rosdi et al., 2011). Moreover, to attain tiny features, which are highly strong to rotation along with a translation, the scale-invariants feature transform (SIFT) (Manickam et al., 2019) was deployed.

Figure 2 Architecture of he-ChOA-CNN

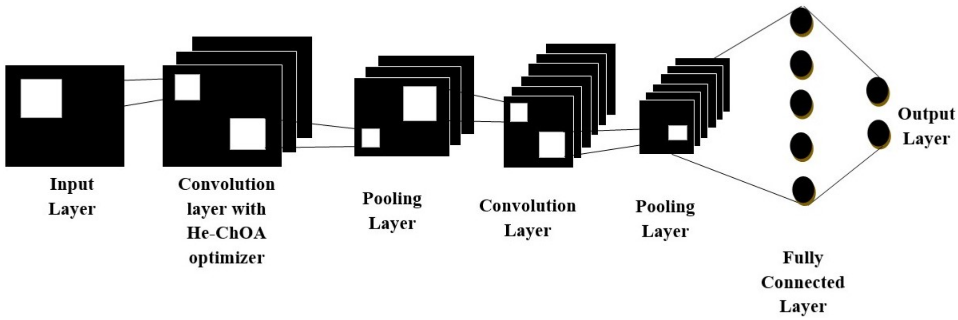

Finally, the extracted features are expressed as:

$$IF(n) = \{IF(1), IF(2), ..., IF(N)\} \tag{22}$$

where $IF(n)$ denotes the extracted features from the synthetic images.

2.7 *Classification*

The 'he-ChOA-CNN' accepts the extracted features as input. A sort of neural network is called CNN wherein the input is converted through a sequence of the layer as of the feature values to the scores. '3' significant layers namely convolution layer (CL), pooling layer (PL), and fully connected layer (FCL) betwixt input and output layer are needed by CNN (Yuan et al., 2014). The parameters called weights and biases of the neurons are encompassed by each layer. Conventionally, the weight values in CNN are arbitrarily generated. Therefore, poor prediction quality of the model is attained with augmented losses. The weights are optimised by utilising the he-initialised chimp optimisation algorithm for lessening the losses and obtaining more precise results. The 'he' initialisation technique is utilised for ameliorating the convergence speed of the ChOA method. Figure 2 illustrates the proposed he-ChOA-CNN architecture.

- *Convolution layer:* The input data is reshaped by the input layer into a D-dimensional matrix. The convolution operation betwixt the inputted features and the weight values (kernels) is performed by the CL. After that, for the ReLU layer, the convoluted output is implemented that returns the rectified feature map (FM) via changing all the negative values to zero. The progress of FM in the CL is formulated mathematically as:

$$O_{Conv}^{fn(n)} = \delta(\Sigma IF(n) * \delta_{wt_n} + \xi) \tag{23}$$

where $O_{Conv}^{fn(n)}$ denotes the FM obtained from the convolution layer, δ denotes the nonlinear activation function (ReLU), δ_{wt_n} denotes the weight values and ξ denotes the bias value given to each FM.

- *Pooling layer:* The size of the inputted FM attained subsequent to convolution and ReLU operations is decreased by this layer. The max-pooling function is applied for dimensionality reduction. The network's computation is quickened by the max-pooling function via identifying the most dominating features. Therefore, the pooled FM of the PL is specified as:

$$O_{pool}^{fn(n)} = \phi_{mp}(O_{Conv}^{fn(n)}) \tag{24}$$

where $O_{pool}^{fn(n)}$ denotes the pooled FM, $\phi_{mp}(.)$ denotes the max-pooling function.

- *Fully connected layer:* The pooled output is flattened into a solo column vector and is implemented to the FCL after the total convolution together with pooling operations. To learn the input features, each neuron in the prior layer is joined to each neuron on the subsequent layer. The input is fed by the FCL to the softmax layer. It employs the softmax function to transmute the input scores into addition of output probabilities. The softmax layer's output is attained as:

$$O_{fc}^{fm(n)} = \delta_{sm}(\Sigma O_{flat}^{fm(n)} * \delta_{wt_n} + \xi) \tag{25}$$

where $O_{fc}^{fm(n)}$ denotes the output of the FCL, δ_{sm} denotes the softmax function, $O_{flat}^{fm(n)}$ denotes the flattened vector, δ_{wt_n} denotes the weight values and ξ denotes the bias value

Lastly, the output images with labels are contained by the output layer. Next, the appraisal of LF is done. Here, the weight values are optimised by the he-ChOA if the target is not matched with that of the observed output. A metaheuristic algorithm enthused via the individual intelligence along with the sexual drive of the chimps is called ChOA. Grounded on the disparate abilities of the chimps (Khishe and Mosavi, 2020) together with their group strategy in updating their parameters, the successful hunt is achieved on a chimp's colony. Chimps population (i.e., the weight values to be optimised) are separated into '4' groups termed driver, barrier, chaser, together with the attacker for the hunting procedure. The driver follows the prey, the barrier blocks the prey's escape route, the chaser moves quickly for catching the prey, and the attacker predicts the escaping route of the prey to attack it. In ChOA, the algorithm's convergence speed is lessened by the random vector utilised for updating the prey's position (Zhang, 2021). The random vector is initialised utilising the he initialisation technique for resolving this issue. The best initialisation strategy is the 'he' initialisation (Datta, 2020). It initialises the values arbitrarily but with variance. The random values are taken by this technique and it outputs the variation of those values approximately to one. For augmenting the convergence rate, this variance calculation is helpful.

In the exploration phase, the competence to explore the prey position via driving, blocking, as well as chasing is possessed by chimps. The initial position of the prey is located centred on the solution updated by the initial attacker, driver, barrier, along with chaser to imitate the chimps' behaviour. Next, the four best solutions attained are stored. The other chimps are forced in updating their positions in the best solution. The best solutions obtained are:

$$D_{n=1,2,3,4} = \begin{cases} D(1) = D_{att} - \alpha_1.r_{att} \\ D(2) = D_{chas} - \alpha_2.r_{chas} \\ D(3) = D_{bar} - \alpha_3.r_{bar} \\ D(4) = D_{driv} - \alpha_4.r_{driv} \end{cases} \tag{26}$$

where D denotes the position vector updated according to $(D_{att}, D_{chas}, D_{bar}, D_{driv})$ denotes the distance vector and α is the dynamic coefficient. The distance vector and coefficient are expressed as:

$$r_{(att,chas,bar,driv)} \\ = \begin{cases} r_att = |\beta * D_{att} - \gamma * D_{chimp}|, \alpha_1 = \zeta_1(2\epsilon_1 - 1) \\ r_chas = |\beta * D_{chas} - \gamma * D_{chimp}|, \alpha_2 = \zeta_2(2\epsilon_1 - 1) \\ r_bar = |\beta * D_{bar} - \gamma * D_{chimp}|, \alpha_3 = \zeta_3(2\epsilon_1 - 1) \\ r_driv = |\beta * D_{driv} - \gamma * D_{chimp}|, \alpha_4 = \zeta_4(2\epsilon_1 - 1) \end{cases} \tag{27}$$

where $\beta = 2\epsilon_2$ and ζ are the coefficients, γ is the Chen chaotic vector.

Then, attack of the prey is done in the exploitation phase, which could be signified by lessening the α value in line with the ζ value. The chimp's subsequent position could be at any point among its current position together with the prey's location when the arbitrary values of α are in the gamut of [1, –1]. The vector determines the convergence for attacking the prey as well as divergence to look for the prey on the exploitation phase, which is initialised utilising the 'he' as:

$$\zeta = y(1, -1) * \sqrt{\frac{2}{y}} \tag{28}$$

where y implies the parameter on the gamut of [1, –1]. The variance of arbitrary values is offered by the 'he'-initialisation in the gamut of [1, –1] approximately to 1 by the parameter called. The algorithm's convergence speed is ameliorated.

Amid the hunting procedure, the chimps quit their responsibilities on account of their sexual motivation. The updating strategy could be performed either by normal behaviour or chaotic behaviour at this stage. It could be specified as:

$$D_{chimp}(i+1) = \begin{cases} D_{pr}(i+1) - \alpha.r & \text{if } \phi < 0.5 \\ \gamma & \text{if } \phi > 0.5 \end{cases} \tag{29}$$

where ϕ ε (0, 1) implies the random vector that finds the updation behaviour. For alleviating the local optima together with slower convergence rate issues, the chimps might be assisted by the chaotic maps. The weight values are optimised.

After training, the testing of the target image is performed with a trained system on the querying step. Here, the gap betwixt the trained system's output and the target is identified. Then, the outcome is returned as an authorised and unauthorised user.

3 Results and discussion

In order to access the effectiveness of the proposed system, numerous experiments are performed in this section. The experiments are conducted using Finger Vein USM (FV-USM) Database (Asaari et al., 2014) which contains a total of 5,904 images from 492 finger classes. For training and testing, 80% of data and 20% of data are employed from this database respectively.The proposed FRS is implemented in the working platform of Python.

3.1 Performance parameters

The efficiency of the proposed technique is analysed based on the metrics such as sensitivity, specificity, false positive rate (FPR), false negative rate (FNR), false discovery rate (FDR), false recognition rate (FRR), Matthew's correlation coefficient (MCC), negative predictive value (NPV), precision, recall, F-score, accuracy, pixel signal to noise ration (PSNR) along with structure similarity index measure (SSIM). These metrics are calculated based on the values obtained from the confusion matrix. In predictive analytics, a confusion matrix is a table with two rows and two columns that report the number of TP, FN, FP, and FN. This permits a more comprehensive investigation than just perceiving the proportion of correct classifications. The performance metrics are evaluated centred on parameters like true positive ($t^{(p)}$), true negative ($t^{(n)}$), false positive ($f^{(p)}$), together with false negative ($f^{(n)}$). For a better system, $f^{(p)}$ should be minimum and $t^{(p)}$ should be maximum.The equations for the performance parameters are mentioned herewith.

3.1.1 Sensitivity

Sensitivity is a performance measure that describes the predictive performance of a classification model. For finger vein recognition, to measure the effectiveness of a proposed system, sensitivity measures the number of authorised finger veins identified correctly that has a positive test result.

$$Sensitivity = \frac{t^{(p)}}{t^{(p)} + f^{(n)}} \tag{30}$$

3.1.2 Specificity

Specificity measures the number of mismatched finger veins (i.e., negative examples) that have a negative test result. The correct identification of mismatched finger veins by using the proposed system shows effective results.

$$Specificity = \frac{t^{(n)}}{f^{(p)} + t^{(n)}} \tag{31}$$

3.1.3 FPR

It is defined as the ratio betwixt the number of negative events wrongly classified as positive (false positives) along with the total number of actual negative events. The lower FPR shows better performance.

$$FPR = \frac{f^{(p)}}{f^{(p)} + t^{(n)}} \tag{32}$$

3.1.4 FNR

It portrays that a finger vein does not match with any of the people when the person actually has the matching results. The lower mismatching shows that the proposed model identifies the person correctly, which shows that the system is more effective in terms of recognition.

$$FNR = \frac{f^{(n)}}{t^{(p)} + f^{(n)}} \tag{33}$$

3.1.5 FDR

FDR is a technique of conceptualising the rate of errors during testing when performing numerous comparisons. The FDR is the expected ratio of the number of FP classifications (false discoveries) to the total number of positive classifications.

$$FDR = \frac{f^{(p)}}{f^{(p)} + t^{(p)}} \tag{34}$$

3.1.6 FRR

The FRR is the gauge of the probability that the biometric security system will erroneously reject access attempt by an authorised user. A system's FRR normally is implied as to the ratio of the number of false recognitions divided by the number of true positives and false negatives.

$$FRR = \frac{f^{(n)}}{t^{(p)} + f^{(n)}} \tag{35}$$

3.1.7 MCC

MCC is a correlation coefficient betwixt the predicted values along with the true values. It returns a value between –1 and +1. When the predictions are perfect, the MCC will be +1 and 0 for the imperfect recognition.

$$MCC = \frac{t^{(p)} \cdot t^{(n)} - f^{(p)} \cdot f^{(n)}}{\left[\left(t^{(p)} + f^{(p)}\right) \cdot \left(t^{(p)} + f^{(n)}\right) \cdot \left(t^{(n)} + f^{(p)}\right) \cdot \left(t^{(n)} + f^{(n)}\right)\right]^{1/2}} \tag{36}$$

3.1.8 NPV

NPV is a proportion of giving negative outcomes. It is defined as the number of TN (people who test negative who does not have a matching finger vein) divided by the total number of the person who assesses negative.

$$NPV = \frac{t^{(n)}}{f^{(n)} + t^{(n)}} \tag{37}$$

3.1.9 Precision

The ratio of true positives to the total predicted positives is termed precision. It is the degree to which a process will repeat the same value.

$$Precision = \frac{t^{(p)}}{f^{(p)} + t^{(p)}} \tag{38}$$

3.1.10 Recall

Recall defines the proportion of correct identification of actual positive results (authorised finger veins). This means that, it measures the percentage of actual finger veins that were correctly classified for recognising a person.

$$Recall = \frac{t^{(p)}}{t^{(p)} + f^{(n)}} \tag{39}$$

3.1.11 Accuracy

A parameter that usually elucidates how the model carries out across all classes is called accuracy. It is helpful when all classes are of equal significance. It is computed as the ratio betwixt the number of correct predictions to the total number of predictions.

$$Accuracy = \frac{t^{(p)}}{t^{(n)} + t^{(s)}} \tag{40}$$

3.1.12 F-score

The F1-score merges the precision along with recall of a classifier into a single metric by taking their harmonic mean. Therefore, both TP and FN are considered in this score.

$$F - score = 2 * \frac{Precision * Recall}{Precision * Recall} \tag{41}$$

3.1.13 PSNR

PSNR is the ratio betwixt the original and compressed image expressed in decibels. This ratio is utilised as a quality measurement betwixt the original and a compressed image. The superior the PSNR, the superior the quality of the compressed or reconstructed image, formulated as:

$$PSNR = 10 \log_{10} \frac{MAX^2}{MSE} \tag{42}$$

where in MAX signifies the maximum possible pixel value of the image and MSE denotes the means square error.

3.1.14 SSIM

A perceptual metric that quantifies image quality degradation engendered by processing like data compression or by losses in data transmission is termed the structural similarity index (SSIM). It is a complete reference metric that needs '2' images from the same image capture such as a reference image along with a processed image.

$$PSNR = 10 \ \log_{10} \frac{MAX^2}{MSE} \tag{43}$$

where μ_x denotes the average of x and μ_y denotes the average of y. The variance of x is denoted by σ_x^2 and the variance of y is denoted by σ_y^2. σ_{xy} denotes the covariance of x and y. c_1, c_2 are the two variables to stabilise the division with weak denominator.

3.2 Performance analysis

The proposed technique's performance is correlated with the prevailing artificial neural network (ANN) (Kumar and Vikram, 2010), deep convolution neural networks (DCNN) (Deshpande et al., 2020), convolution neural networks (CNN) (Wong and Lai, 2020), recurrent neural networks (RNN) (Ackerson et al., 2020) and generative adversarial networks-based CNN (GAN_CNN) to authenticate the efficiency of the proposed WS-progressive-GAN-based he-CHOA-CNN methodology centred on some quality metrics. On the grounds of pixel signal to noise ration (PSNR) and SSIM, the performance of the proposed RCLAHE and existing contrast limited adaptive histogram equalisation (CLAHE) (Vidyarthi and Malik, 2021), histogram (Liang et al., 2012), along with Gaussian filtering (Khan et al., 2017) is examined. The proposed he-ChOA, along with prevailing ChOA (Khishe and Mosavi, 2020), crow search optimisation (CSO) (Hussien et al., 2020), rat swarm optimisation (RSO) (Dhiman et al., 2020), and Harish Hawks optimisation (HHO) (Heidari et al., 2019) techniques, are then subjected to fitness vs. iterations study.

Figure 3 Performance analysis of proposed and existing methods based on sensitivity, specificity and accuracy (see online version for colours)

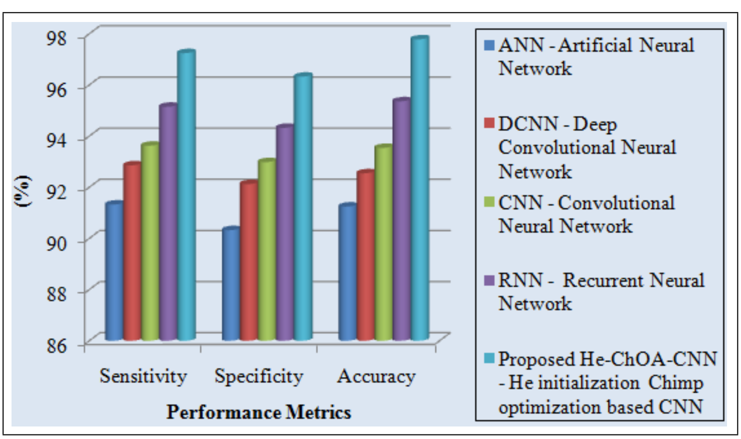

3.2.1 *Performance analysis of generative adversarial networks-based CNN (GAN_CNN)*

The sensitivity, specificity, along with the accuracy of the prevailing along with proposed techniques is assessed in Figure 3. The most vital parameters like sensitivity, specificity and accuracy are reliant on true-positive (TP), true-negative (TN), false-positive (FP) and false-negative (FN). The sensitivity of prevailing methodologies like ANN has 91.3256, DCNN has 92.8574, CNN has 93.6258, RNN has 95.1485, and GAN_CNN has 96.1863, which are smaller than the proposed technique, that is, 97.2458. The proposed method has greater specificity and accuracy values of 96.3258 and 97.78459 respectively. On comparing with the proposed technique, the prevailing model accomplishes lesser specificity and accuracy. Therefore, the enrichment made in the proposed techniques effectively acknowledges the FV than the prevailing methodologies, and also it is evident from the aforesaid investigation.

Figure 4 Performance analysis of proposed and existing methods based on precision, recall and F-measure (see online version for colours)

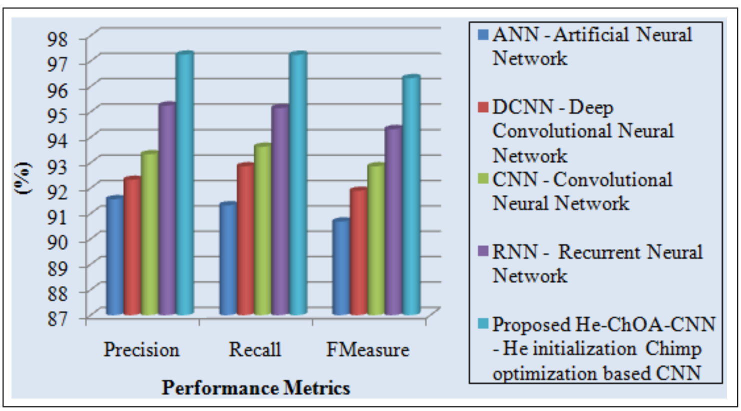

Figure 5 Performance analysis of proposed and existing methods based on MCC, NPV and FPR (see online version for colours)

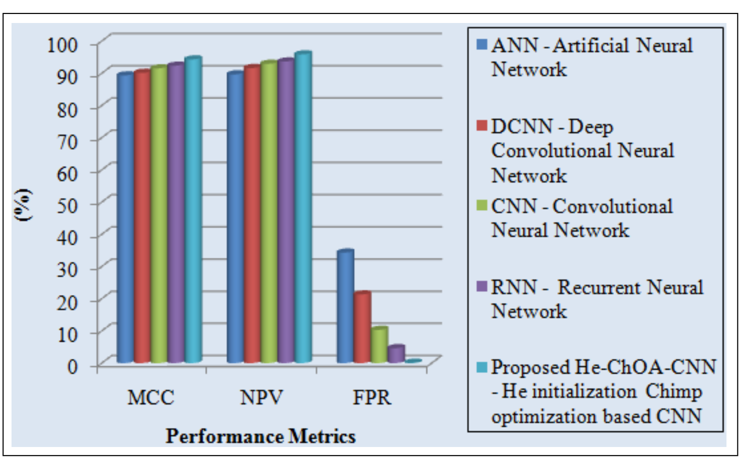

Figure 6 Performance analysis of proposed and existing methods based on FNR, FRR and FDR (see online version for colours)

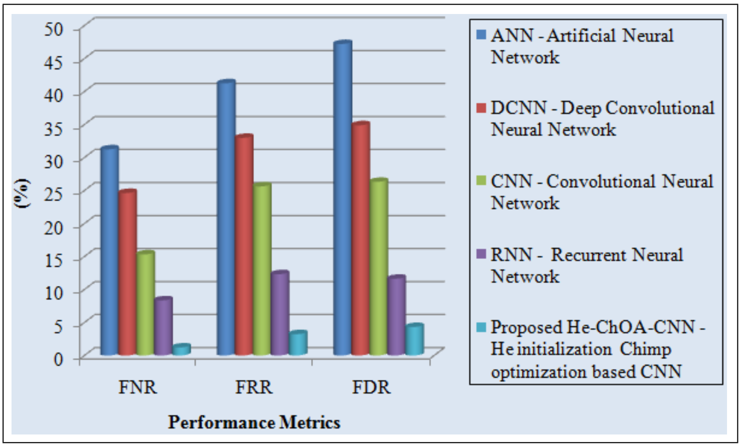

On basis of precision, recall, and F-measure, the proposed and prevailing technique's performance is exhibited in Figure 4. The metric that measures how many correct positive forecasts have been made is termed precision. The percentage of total appropriate outcomes accurately categorised by the algorithm is called recall. For generating a single score that accounts for both precision and recalls concerns in a single number, F-measure is used. The precision and recall of the prevailing ANN, DCNN, CNN, RNN and GAN_CNN are 91.5633 and 91.3256, 92.3254 and 92.8574, 93.3322 and 93.6258, 95.2477 and 95.1485, and 96.0285 and 96.1863. The Precision and Recall for the proposed method achieve greater values, such as 97.2547 and 97.2458. The proposed work has good performance than the prevailing techniques concerning F-measure. The proposed work is superior to the prevailing techniques, as evident from the preceding analysis.

Centred on the MCC, NPV, and FPR, the proposed and prevailing technique's performance are evaluated in Figure 5. The NPV calculates how many of all negative forecasts were correct. With the predicted classes, the MCC measures the true classes. The prevailing, DCNN, CNN, RNN, and GAN_CNN have MCC of 89.3322, 90.1245, 91.5478, 92.3647, and 93.1794, but the proposed technique has an MCC of 94.3265. On comparing with the prevailing techniques, the proposed one has a greater value of MCC. When analogised to the proposed approach, existing ANN and DCNN have lesser performance, while existing CNN and RNN have medium performance regarding NPV. The FPR value acquired from the proposed is 0.1247, and it is extremely smaller than the prevailing techniques. Therefore, the proposed technique produces better outcomes than the prevailing approach.

The proposed together with the prevailing technique's FNR, FRR, and FDR are exhibited in Figure 6. For the system to work well, the negative measures like FNR, FRR, and FDR should be less as possible. The proposed one has decreased the FNR, FRR, and FDR values to 1.2254, 3.2478, and 4.3257 respectively. FNR, FRR, and FDR have the largest values for ANN and DCNN, and they are 31.2487 and 24.6325, 41.2589 and 32.9854, and 47.21245 and 34.89565 respectively in the prevailing approaches. Thus, the proposed strategy produces superior outcomes for all metrics than the prevailing techniques, and also it is clear from the above analysis.

3.2.2 Performance analysis of proposed RCLAHE method

The PSNR of the proposed and prevailing approaches is illustrated in Figure 7. The proposed technique achieves a PSNR of 30.01731%, while the CLAHE has 9.48688%, histogram has 14.87275%, and Gaussian filtering has 19.26135% in the prevailing model. Thus, the proposed methodology outperforms the prevailing techniques on account of the enrichment. Therefore, the proposed model improves image contrast more efficiently than the prevailing methodologies.

Figure 7 Performance analysis of proposed RCLAHE with existing methods based on PSNR (see online version for colours)

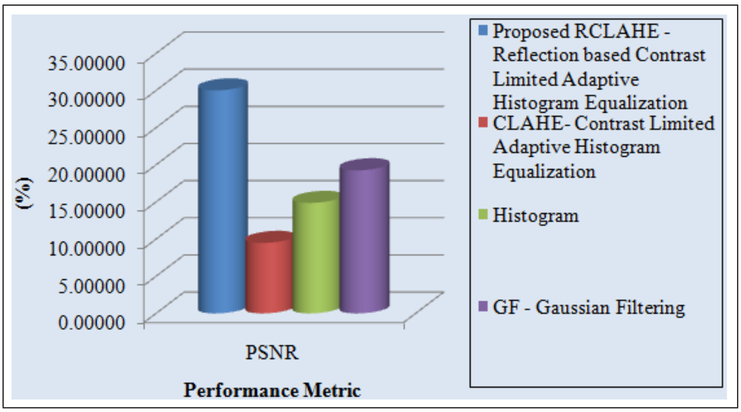

Figure 8 Performance analysis of proposed RCLAHE with existing methods based on SSIM (see online version for colours)

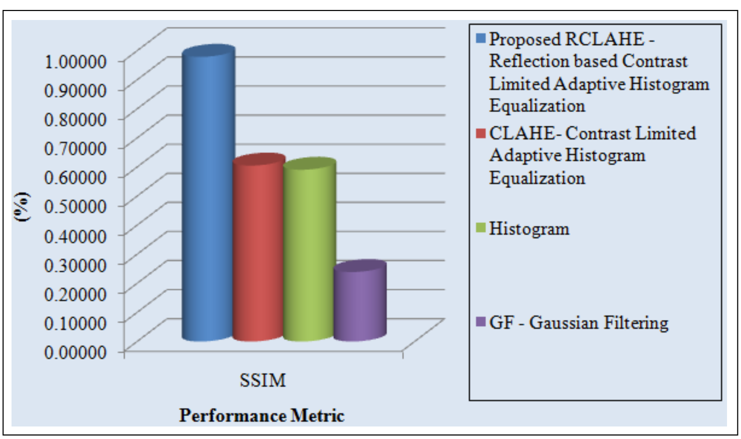

Centred on SSIM, the performances of the proposed and prevailing methodologies are depicted in Figure 8. The prevailing CLAHE, histogram, and Gaussian filtering have an average SSIM of 0.60501, 0.59066, and 0.89233. However, on comparison with the prevailing techniques, the RCLAHE achieves an average of 0.97897 SSIM which is higher. Thus, in contrast to the prevailing techniques, the proposed work performs better.

3.2.3 Performance analysis of proposed ChOA

The total iterations engaged for the analysis differ as 10, 20, 30, 40, and 50, which is exhibited in Figure 9. The prevailing techniques like ChOA, CSO, RSO and HHO have the fitness value of 74.3256, 62.32568, 54.6532, and 48.32459 respectively, whereas the proposed model accomplishes 89.3256 of fitness value, for the ten iterations. In the proposed technique for the remaining 20 iterations, 30 iterations, 40 iterations, and 50 iterations, the fitness values are 102.3256, 112.4578, 124.3256, and 132.1245 respectively. Hence, for the diverse number of iterations the prevailing models have lesser fitness value in relation to the He-ChoA technique.

Figure 9 Performance analysis of proposed ChOA (see online version for colours)

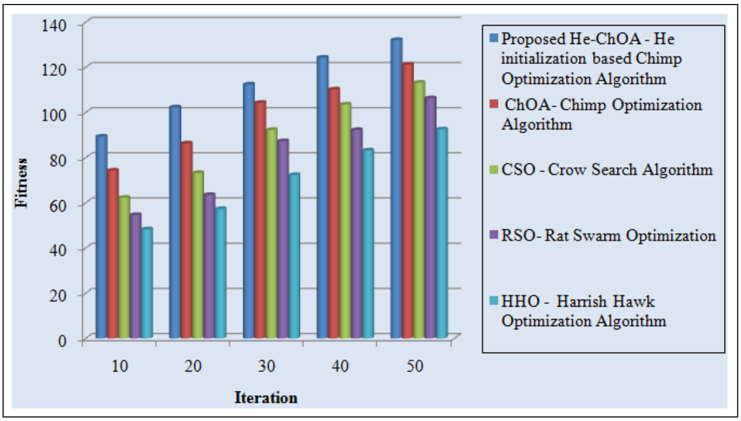

Figure 10 Computational cost analysis (see online version for colours)

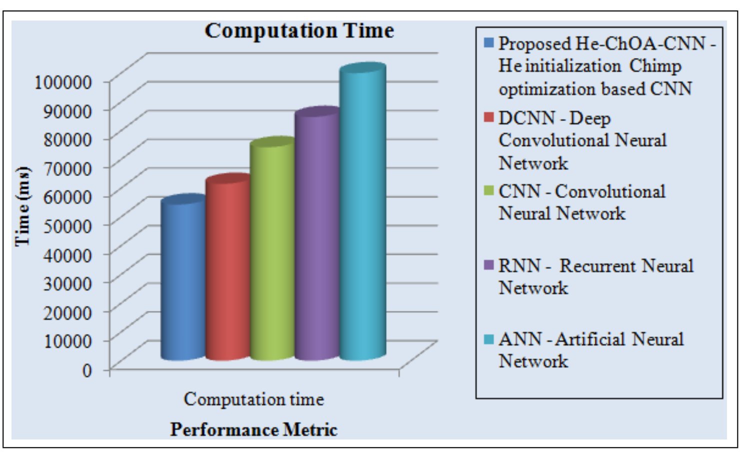

Figure 10 shows the computational cost of the proposed work with prevailing works. The proposed work attains computation time that is lesser than the values attained by the prevailing works. The computation time attained by the proposed he-ChOA-CNN technique is 54,302 ms, whereas existing DCNN, CNN, RNN, and ANN are, 61,481 ms, 74,238 ms, 84,756 ms and 99,991 ms. By comparing the computation time of the proposed and existing model, the proposed one outperforms the other existing technique by showing less time than the others. Therefore, it is guaranteed that the proposed system achieves more efficient performance than others.

Figure 11 Training and testing time analysis (see online version for colours)

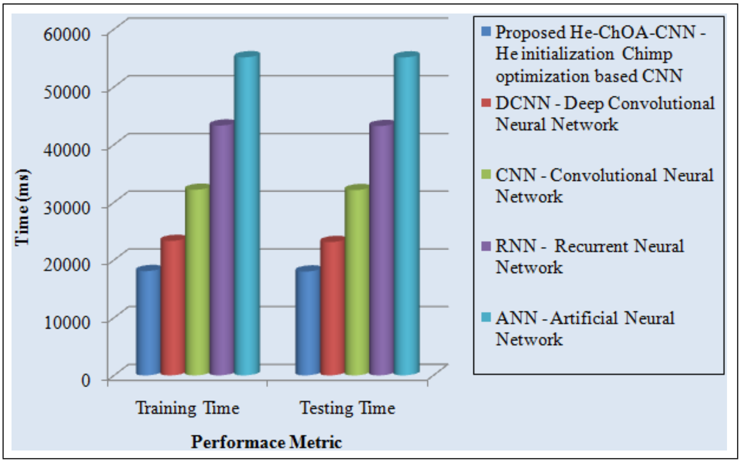

Figure 12 Accuracy analysis of proposed classifier (see online version for colours)

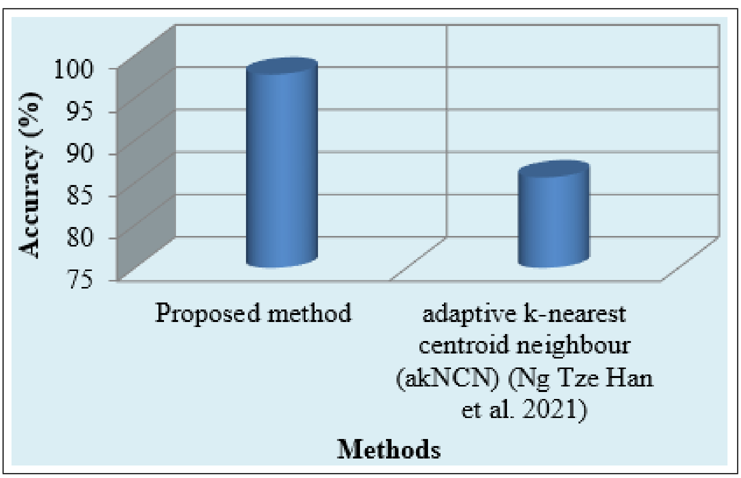

Figure 11 depicts the training and testing times of the proposed methodology and the prevailing works. The proposed technique attained the training and testing time of 18,070 ms and 18,000 ms which are lower than the prevailing methods. The existing techniques require the training time of 23,299 ms (DCNN), 32,165 ms (CNN), 43,290 ms (RNN), and 55,120 ms (ANN). Also, the testing time taken by the proposed system to recognise the authority of finger veins is, 23,100 ms, 32,105 ms, 43,209 ms, and 55,101 ms for DCNN, CNN, RNN, and ANN respectively. When analogised to the prevailing techniques, the training and testing time of the proposed system is lower. The superior outcomes of the proposed technique show the improvement in the proposed model's efficiency.

To reiterate the performance of the proposed classifier, it is compared with the adaptive k-nearest centroid neighbour (akNCN) (Rosdi et al., 2011) in terms of accuracy. The comparison is depicted in the form of Figure 12. The proposed classifier attains the value of 97.78% while the existing work acquires the value of 85.64%. The superior results of the proposed method show the efficiency of the improvements made in this work.

4 Conclusions

An efficient FV recognition system for authentication is proposed. Presenting an effectual FP reconstruction system using a WS_progressive GAN and he-ChOA-CNN classifier is the main goal here. Seven phases are there in the proposed work. The data gathered as of the publicly available dataset is employed for analysing the proposed model's performance. Concerning the accuracy, precision, recall, F-measure, sensitivity, specificity, NPV, FNR, MCC, FRR, FDR and FPR, the proposed he-ChOA-CNN's performance is analogised to the ANN, DCNN, CNN and RNN. High performance is obtained by the proposed work for all metrics. The recognition accuracy of 97.78459 is attained by the he-ChOA-CNN. Analogised to the prevailing methods, the analysis proves that the proposed scheme and its efficiency for recognising the identity of the person utilising FV are better. In the future, more advanced algorithms can well be incorporated in the proposed work for improving performance.

References

Ackerson, J.M., Dave, R. and Seliya, N. (2020) 'Applications of recurrent neural network for biometric authentication & anomaly detection', *Information*, Vol. 12, No. 7, p.272.

Asaari, M.S.M., Suandi, S.A. and Rosdi, B.A. (2014) 'Fusion of band limited phase only correlation and width centroid contour distance for finger based biometrics', *Expert Systems with Applications*, Vol. 41, No. 7, pp.3367–3382.

Dai, H., Pears, N. and Smith, W. (2020) 'A data-augmented 3D morphable model of the ear', *IEEE International Conference on Automatic Face & Gesture Recognition (FG 2018)*, pp.404–408.

Datta, L. (2020) *A Survey on Activation Functions and their Relation with Xavier and He Normal Initialization*, arXiv preprint arXiv:2004.06632.

Deshpande, U.U., Malemath, V.S., Patil, S.M. and Chaugule, S.V. (2020) 'End-to-end automated latent fingerprint identification with improved DCNN-FFT enhancement', *Frontiers in Robotics and AI*, Vol. 7, No. 2296-9144, p.166.

Dhiman, G., Garg, M., Nagar, A., Kumar, V. and Dehghani, M. (2020) 'A novel algorithm for global optimization: rat swarm optimizer', *Journal of Ambient Intelligence and Humanized Computing*, Vol. 12, No. 8, pp.8457–8482.

Fairuz, S., Habaebi, M.H. and Elsheikh, E.M.A. (2019a) 'Pre-trained based CNN model to identify finger vein', *Bulletin of Electrical Engineering and Informatics*, Vol. 8, No. 3, pp.855–862.

Fairuz, S., Habaebi, M.H. and Elsheikh, E.M.A. (2019b) 'Adaptive learning Gabor filter for finger-vein recognition', *IEEE Access*, Vol. 7, No. 2950698, pp.159821–159830.

Heidari, A.A., Mirjalili, S., Faris, H., Aljarah, I., Mafarja, M. and Chen, H. (2019) 'Harris Hawks optimization: algorithm and applications', *Future Generation Computer Systems*, Vol. 97, No. 0167-739X, pp.849–872.

Hu, N., Ma, H. and Zhan, T. (2020) 'Finger vein biometric verification using block multi-scale uniform local binary pattern features and block two-directional two-dimension principal component analysis', *Optik*, Vol. 208, No. 0030-4026, p.163664.

Huang, X., Qian, P. and Liu, M. (2020) 'Latent fingerprint image enhancement based on progressive generative adversarial network', *Proceedings of the IEEE/CVF Conference on Computer Vision and Pattern Recognition Workshops*, pp.800–801.

Hussien, A.G., Amin, M., Wang, M., Liang, G., Alsanad, A., Gumaei, A. and Chen, H. (2020) 'Crow search algorithm: theory, recent advances, and applications', *IEEE Access*, Vol. 8, No. 2169-3536, pp.173548–173565.

Kapoor, K., Rani, S., Kumar, M., Chopra, V. and Brar, G.S. (2021) 'Hybrid local phase quantization and grey wolf optimization based SVM for finger vein recognition', *Multimedia Tools and Applications*, Vol. 80, No. 10, pp.15233–15271.

Khan, T.M., Bailey, D.G., Khan, M.A. and Kong, Y. (2017) 'Efficient hardware implementation for fingerprint image enhancement using anisotropic Gaussian filter', *IEEE Transactions on Image processing*, Vol. 26, No. 5, pp.2116–2126.

Khishe, M. and Mosavi, M.R. (2020) 'Chimp optimization algorithm', *Expert Systems with Applications*, Vol. 149, No. 0957-4174, p.113338.

Kirchgasser, S., Kauba, C., Lai, Y.L., Zhe, J. and Uhl, A. (2020) 'Finger vein template protection based on alignment-robust feature description and index-of-maximum hashing', *IEEE Transactions on Biometrics, Behavior, and Identity Science*, Vol. 2, No. 4, pp.337–349.

Kumar, R. and Vikram, B.D. (2010) 'Fingerprint matching using multi-dimensional ANN', *Engineering Applications of Artificial Intelligence*, Vol. 23, No. 2, pp.222–228.

Lai, Y., Jin, Z., Wong, K. and Tistarelli, M. (2021) 'Efficient known-sample attack for distance-preserving hashing biometric template protection schemes', *IEEE Transactions on Information Forensics and Security*, Vol. 16, No. 1556-6021, pp.3170–3185.

Liang, K., Ma, Y., Xie, Y., Zhou, B. and Wang, R. (2012) 'A new adaptive contrast enhancement algorithm for infrared images based on double plateaus histogram equalization', *Infrared Physics & Technology*, Vol. 55, No. 4, pp.309–315.

Liu, H., Yang, G., Yang, L. and Yin, Y. (2019a) 'Learning personalized binary codes for finger vein recognition', *Neurocomputing*, Vol. 365, pp.62–70.

Liu, C.Y., Ruan, S.J., Lai, Y.R. and Yao, C.Y. (2019b) 'Finger-vein as a biometric-based authentication', *IEEE Consumer Electronics Magazine*, Vol. 8, No. 6, pp.29–34.

Lu, Y., Yoon, S., Wu, S. and Park, D.S. (2018) 'Pyramid histogram of double competitive pattern for finger vein recognition', *IEEE Access*, Vol. 6, pp.56445–56456.

Lu, H., Du, M., Qian, K., He, X. and Wang, K. (2021) 'GAN-based data augmentation strategy for sensor anomaly detection in industrial robots', *IEEE Sensors Journal*, Vol. 22, No. 18, pp.17464–17474.

Manickam, A., Devarasan, E., Manogaran, G., Priyan, M.K., Varatharajan, R., Hsu, C.H. and Krishnamoorthi, R. (2019) 'Score level based latent fingerprint enhancement and matching using SIFT feature', *Multimedia Tools and Applications*, Vol. 78, No. 3, pp.3065–3085.

Meng, X., Xi, X., Li, Z. and Zhang, Q. (2020) 'Finger vein recognition based on fusion of deformation information', *IEEE Access*, Vol. 8, No. 2169-3536, pp.50519–50530.

Muthusamy, D. and Rakkimuthu, P. (2021a) 'Steepest deep bipolar cascade correlation for finger-vein verification', *Applied Intelligence*, Vol. 52, No. 4, pp.3825–3845.

Muthusamy, D. and Rakkimuthu, P. (2021b) 'A hybridized modified densenet deep architecture with CLAHE algorithm for humpback whale identification and recognition', *Multimedia Tools and Applications*, Vol. 81, No. 14, pp.19779–19793.

Noh, K.J., Choi, J., Hong, J.S. and Park, K.R. (2020) 'Finger-vein recognition based on densely connected convolutional network using score-level fusion with shape and texture images', *IEEE Access*, Vol. 8, No. 2169-3536, pp.96748–96766.

Ramachandra, R., Raja, K.B., Venkatesh, S.K. and Busch, C. (2019) 'Design and development of low-cost sensor to capture ventral and dorsal finger vein for biometric authentication', *IEEE Sensors Journal*, Vol. 19, No. 15, pp.6102–6111.

Ren, H., Sun, L., Guo, J., Han, C. and Wu, F. (2021) 'Finger vein recognition system with template protection based on convolutional neural network', *Knowledge-Based Systems*, Vol. 227, No. 0950-7051, p.107159.

Rosdi, B.A., Shing, C.W. and Suandi, S.A. (2011) 'Finger vein recognition using local line binary pattern', *Sensors*, Vol. 11, No. 12, pp.11357–11371.

Song, J.M., Kim, W. and Park, K.R. (2019) 'Finger-vein recognition based on deep DenseNet using composite image.', *IEEE Access*, Vol. 7, No. 2169-3536, pp.66845–66863.

Tüű-Szabó, B., Kovács, G., Földesi, P., Nagy, S. and Kóczy, L.T. (2021) 'Local binary pattern-based fingerprint matching', *Computational Intelligence and Mathematics for Tackling Complex Problems 3, Studies in Computational Intelligence*, Springer, Vol. 959, pp.183–188.

Wong, W.J. and Lai, S.H. (2020) 'Multi-task CNN for restoring corrupted fingerprint images', *Pattern Recognition*, Vol. 101, No. 0031-3203, p.107203.

Xie, C. and Kumar, A. (2019) 'Finger vein identification using convolutional neural network and supervised discrete hashing', *Pattern Recognition Letters*, Vol. 119, No. 0167-8655, pp.148–156.

Yang, W., Luo, W., Kang, W., Huang, Z. and Wu, Q. (2020) 'FVRAS-Net: an embedded finger-vein recognition and AntiSpoofing system using a unified CNN', *IEEE Transactions on Instrumentation and Measurement*, Vol. 69, No. 11, pp.8690–8701.

Yuan, C., Xia, Z., Jiang, L., Cao, Y., Wu, Q.J. and Sun, X. (2014) 'Fingerprint liveness detection using an improved CNN with image scale equalization', *IEEE Access*, Vol. 7, No. 2169-3536, pp.26953–26966.

Zhang, J., Lu, Z., Li, M. and Wu, H. (2019) 'GAN-based image augmentation for finger-vein biometric recognition', *IEEE Access*, Vol. 7, No. 2169-3536, pp.183118–183132.

Zhang, Y. (2021) 'Chaotic neural network algorithm with competitive learning for global optimization', *Knowledge-Based Systems*, Vol. 231, No. 0950-7051, p.107405.

Zhao, D., Ma, H., Yang, Z., Li, J. and Tian, W. (2020) 'Finger vein recognition based on lightweight CNN combining center loss and dynamic regularization', *Infrared Physics & Technology*, Vol. 105, No. 1350-4495, p.103221.